DE-FG07-07ID14771

The University of New Mexico

A Generalized Boltzmann Fokker-Planck Method for Coupled Charged Particle Transport

Anil K. Prinja, PI

1 Introduction

The goal of this project was to develop and investigate the performance of reduced-physics formulations of high energy charged particle (electrons, protons and heavier ions) transport that are computationally more efficient than not only analog Monte Carlo methods but also the established condensed history Monte Carlo technique. Charged particles interact with matter by Coulomb collisions with target nuclei and electrons, by bremsstrahlung radiation loss and by nuclear reactions such as spallation and fission. Of these, inelastic electronic collisions and elastic nuclear collisions are the dominant cause of energy-loss straggling and angular deflection or range straggling of a primary particle. These collisions are characterized by extremely short mean free paths (sub-microns) and highly peaked, near-singular differential cross sections about forward directions and zero energy loss, with the situation for protons and heavier ions more extreme than for electrons. For this reason, analog or true-physics single-event Monte Carlo simulation, while possible in principle, is computationally prohibitive for routine calculation of charged particle interaction phenomena.

The widely used alternative to analog simulation is the condensed history method [1] where large numbers of collisions are effectively grouped together to create macroscopic collisions. While this improves computational efficiency, the practical implementation of this algorithm exacts a price, namely the sacrifice of correct transport mechanics, which places inherent limitations on the method. In particular, the use of precomputed infinite medium multiple scattering and multiple ionization theories to describe angular deflections and energy-loss straggling at the end of macroscopic steps of prescribed lengths introduces an irreducible systematic or deterministic error in addition to the statistical error associated with the simulation. Moreover, the method breaks down in the vicinity of material interfaces where the precomputed distributions are not valid. The method is typically retrofitted with various corrections that are difficult to generalize to realize systematic improvements in accuracy. In this research, we have developed and demonstrated, in extensive numerical implementations, a computationally efficient and accurate alternative to the condensed history Monte Carlo method for energetic charged particles. The focus has been on developing an improved method to handle extreme physics interactions associated with charged particles, specifically highly peaked elastic nuclear and inelastic electronic scattering, but as a serendipitous side outcome we also developed and demonstrated an efficient multigroup method for coupled proton-neutron transport using MCNPX with purely forward and forward-adjoint approaches. In the latter, a novel forward-adjoint coupling was introduced and applied to the challenging problem of secondary neutron dose resulting from interactions of high energy primary protons. The methodology and results for the multigroup approach have been described in previous progress reports and publications and was not the primary focus of this grant. In this report, we describe the methodology developed for handling extremely peaked scattering and energy losses in Coulomb collisions and itl numerical implementation. One highlight of this work was the implementation of a new energy-loss straggling method directly in the MCNP code. The report concludes with a list of publications and invited seminars resulting from this grant.

2 Generalized Boltzmann Fokker-Planck Approach

A key feature of our algorithm is that it is optimal for implementation in a single-event Monte Carlo simulation and is computationally considerably less costly than the intractable analog single-event simulation. Unlike the condensed history employed in the ITS , EGS4, MCNP/MCNPX, and GEANT production codes, our approach has rigorous transport theoretic foundations and hence does not suffer from the same limitations. We have been guided in the development of our approach by the over-arching philosophy that any new method should be:

- *physically sound* the underlying physics must reflect the analog processes
- *mathematically robust* it should retain the transport theoretic basis of the analog formulation and hence will preserve the correct transport mechanics
- *computationally efficient* it should be characterized by longer mean free paths and less peaked differential cross sections than analog
- *accurate* - it should be possible to incorporate physics model refinements without necessitating changes to algorithm
- *systematic* the methodology should allow accuracy to approach analog

Key to our approach is the idea of regularizing the near singular collision operators in the linear Boltzmann equation for the space-energy-angle distribution function, that describe the energy loss and scattering (angular deflection) interactions and which are the underlying cause of the inefficiency in the analog simulation of these processes. In our method, the analog problem is replaced with an approximate one, a pseudo-transport problem, which preserves important projections of analog scattering and energy loss interaction physics and approximates rather than neglects the higher order contributions. Hence our model is appropriately described as a reduced-physics model.

By developing methods that enable this conservation principle to be systematically applied, the above delineated attributes can be realized in a robust algorithm. Significantly, by shifting dependence of the method away from detailed prescriptions of the physical interactions and emphasizing instead a finite set of projections of these processes, the regularization procedure becomes particle independent. That is, computational efficiency and accuracy can be realized for all charged particles interacting through Coloumb forces. Our approach is based on systematic preservation of moments of the underlying differential cross sections using discrete, continuous and hybrid models and the motivation for this resides in the differential approximations to the collision operators made possible by the peaked cross sections. In particular, we build on Fokker-Planck and Boltzmann Fokker-Planck approximations and we accordingly refer to our new formulation as the Generalized Boltzmann Fokker-Planck or GBFP method.

3 Moment-Preserving Models

We consider an electron beam incident on a slab of material. The angular flux $\psi(\vec{r},\vec{\Omega},E)$ of electrons at spatial location $\vec{r}(x,y,z)$ traveling along direction $\vec{\Omega}(\mu,\phi)$ with energy E satisfies the linear transport equation,

$$\vec{\Omega}\cdot\nabla\psi(\vec{r},\vec{\Omega},E)=\int_0^\infty\int_{4\pi}\sigma_s(\vec{r},\vec{\Omega}\cdot\vec{\Omega}',E'\rightarrow E)\,\psi(\vec{r},\vec{\Omega}',E')d\vec{\Omega}'dE'-\sigma_s(\vec{r},E)\,\psi(\vec{r},\vec{\Omega},E), \quad (1)$$

where $\sigma_s(\vec{r},\vec{\Omega}\cdot\vec{\Omega}',E'\rightarrow E)$ is the differential scattering cross section and $\sigma_s(\vec{r},E)$ is the total scattering cross section. We consider a monoenergetic pencil beam incident on the left face along the z-axis with zero incidence on the right face,

$$\psi(x,y,0,\mu,\phi,E)=\frac{1}{2\pi}\delta(\mu-1)\,\delta(E-E_0)\,\delta(x)\,\delta(y),\quad \mu>0, \quad (2)$$

$$\psi(x,y,Z,\mu,\phi,E)=0,\quad \mu<0. \quad (3)$$

In electron interactions with target atoms, elastic and inelastic interactions are treated independently. Furthermore, we assume that elastic collisions occur without energy loss and inelastic collisions occur without angular deflection. Under these conditions, the transport equation becomes,

$$\begin{aligned}\vec{\Omega}\cdot\nabla\psi(\vec{r},\vec{\Omega},E) &= \int_{4\pi}\sigma_{s,el}(\vec{r},\vec{\Omega}\cdot\vec{\Omega}',E)\,\psi(\vec{r},\vec{\Omega}',E)d\vec{\Omega}'\\ &+ \int_0^\infty\sigma_{s,in}(\vec{r},E'\rightarrow E)\,\psi(\vec{r},\vec{\Omega},E')dE'\\ &- [\sigma_{s,el}(\vec{r},E)+\sigma_{s,in}(\vec{r},E)]\,\psi(\vec{r},\vec{\Omega},E). \end{aligned}\quad (4)$$

where $\sigma_{s,el}$ is the elastic scattering cross section and $\sigma_{s,in}$ is the inelastic scattering cross section. The elastic scattering differential cross section (DCS) is accurately described by the Mott cross section at high energies and correspondingly by the Möller cross section for inelastic interactions [2]. As mentioned previously, these differential cross sections are highly peaked about the forward direction ($\vec{\Omega}\cdot\vec{\Omega}'\equiv\mu_0=1$) and small energy-loss ($E'-E=0$) while the total scattering cross section is large ($\sigma_s(\vec{r},E)\gg 1$). The high frequency of electron collisions with target atoms, coupled with miniscule changes in the electron state per collision, is the underlying cause of the inefficiency of analog electron Monte Carlo simulations. In the next section we describe our reduced transport model based on moment-preserving discrete scattering representations, which is demonstrated in subsequent sections to be a practical alternative to analog Monte Carlo calculations of electron dose and comparable to condensed history methods in computational efficiency.

3.1 Angular Scattering

To introduce our approach to angular scattering, we define *momentum transfer* moments of the elastic DCS according to

$$\sigma_{n,el}(\vec{r},E)\equiv 2\pi\int_{-1}^{1}d\mu_0\,(1-\mu_0)^n\sigma_{s,el}(\vec{r},\mu_0,E),\quad n=1,2,\ldots \quad (5)$$

Note that unlike the traditional Legendre moments, the momentum transfer moments $\sigma_{n,el}$ are all positive for a positive DCS, and for a sufficiently peaked DCS, they form a rapidly decreasing sequence. Thus, in a sense (made more precise below) the $\sigma_{n,el}$ provide a natural characterization of forward-peaked scattering, as the Legendre moments do for nearly isotropic scattering. We also note that $\sigma_{1,el}$ is the familiar transport cross section.

The essence of our method is to replace $\sigma_{s,el}(\vec{r}, \mu_0, E)$ by an approximate DCS, $\tilde{\sigma}_{s,el}(\vec{r}, \mu_0, E)$, defined such that the associated momentum transfer moments $\tilde{\sigma}_{n,el}$ are identical to the exact moments $\sigma_{n,el}$ for $n = 1, 2 \ldots N$, where N is arbitrary but finite. All higher moments $\{\tilde{\sigma}_{n,el},\ n = N+1, N+2 \ldots\}$ are approximated in terms of these lower moments. The motivation and expectation is that by not rigorously preserving all momentum transfer moments we are modeling a less singular scattering process. The consequence is that the reduced physics should yield a longer mean free path (mfp) than the actual mfp as well as a less peaked angular-scattering distribution. On the other hand, strictly preserving a number of low-order moments should provide accuracy. This approach was motivated by the observation that the Fokker-Planck approximation to the elastic scattering operator (i) only preserves the first moment $\sigma_{1,el}$ yet is extensively used for pencil beams, forming the basis of the well-known Fermi and Fermi-Eyges solutions, and (ii) constitutes the lowest order in a Generalized Fokker-Planck (GFP) expansion whose coefficients depend on the $\sigma_{n,el}$, $n \geq 1$ [3, 4, 5]. Moreover, Lewis theory [6] clearly demonstrates a direct correlation between preserving moments of the DCS and the accuracy of the model as measured by space-angle moments of the infinite medium solution. This suggests that increasingly more accurate physics can be captured by preserving increasingly higher-order moments. In fact, preserving two moments of the DCS, results in the preservation of all second-order (and first-order) space-angle moments of the particle flux. However, it has been shown [4] that the GFP expansion is asymptotic, being unstable to truncation orders beyond Fokker-Planck. Higher-order moments cannot, therefore, be preserved by retaining only a finite number of terms in this expansion. An alternative approach has been presented [5] where the GFP expansion was first renormalized to yield a convergent series and then converted by resummation to an integral scattering operator possessing a smoother scattering kernel. However, this alternative does not yield an explicit, effective differential cross section. Rather, it gives the coefficients of a spherical harmonics expansion of the cross section.

We adopt a conceptually simpler approach in which $\tilde{\sigma}_{s,el}$ is represented as a superposition of discrete scattering angles,

$$\tilde{\sigma}_{s,el}(\vec{r}, \mu_0, E) = \sum_{l=1}^{L} \frac{\alpha_l(\vec{r}, E)}{2\pi} \delta\left[\mu_0 - \xi_l(\vec{r}, E)\right]. \tag{6}$$

The scattering amplitudes $\{\alpha_l,\ l = 1, 2 \ldots\ L\}$ and scattering cosines $\{\xi_l,\ l = 1, 2 \ldots\ L\}$ are constrained to yield the exact first $2L$ momentum transfer moments $\{\tilde{\sigma}_{l,el} = \sigma_{l,el},\ l = 1, 2 \ldots 2L\}$ as given by Eq.(5). This condition yields a nonlinear algebraic system for the α_l and ξ_l that can be solved using Newton iteration. Sampling precalculated scattering angles using Eq.(6) is almost trivial, which is an important consideration in the overall efficiency of Monte Carlo simulations.

It should be noted that the approximation of angular scattering kernels by discrete angle representations has been proposed and implemented by others previously. In the code

MORSE [7], a discrete representation based on Gaussian quadrature was introduced that exactly preserved the total scattering cross section, $\sigma_{0,el}$. Sloan [8] and Morel [9] refined the MORSE algorithm into an alternative method for solving Eq.(6) by employing Radau quadrature. The method initially preserves the $\sigma_{0,el}$ moment, but then the straight-ahead direction from the quadrature is discarded. The remaining directions and renormalized weights provide an identical solution to Eq.(6) as solving by Newton iteration. Sloan's method has been observed to be robust for a wide range of physics (including the highly forward-peaked elastic scattering of 100 MeV electrons in hydrogen) and $L \leq 8$. An implementation of Sloan's algorithm with an associated Fokker-Planck approximation is described by Morel et al. [9]. We omit the associated Fokker-Planck approximation in our implementation so that higher-order moments may be exactly preserved. We also omit discussion of the pure Fokker-Planck approximation as it was found to be expensive and in any case inaccurate for pencil beam applications.

For $L = 1$, only the transport cross section $\sigma_{1,el}$ and the mean square momentum transfer $\sigma_{2,el}$ are rigorously preserved, but for extremely forward-peaked scattering this may prove sufficient. Notice, in this case, that if the limit $\xi_1 \to 1$ is taken while simultaneously enforcing the requirement that the correct transport cross section be obtained, the Fokker-Planck approximation is realized. Setting ξ_1 close to unity then gives Morel's discrete representation of the Fokker-Planck approximation [9], which provides a practical method for simulating Fokker-Planck scattering by Monte Carlo.

The mfp corresponding to L discrete directions is given by $\tilde{\lambda}_L = \left(\sum_{l=1}^{L} \alpha_l\right)^{-1}$ and can be used as a measure of the potential speed-up over the analog case. For illustration, we consider 1 MeV electrons incident on a gold target with elastic scattering described by the screened Rutherford DCS [10]. The screening parameter at this energy is $\eta = 4.88 \times 10^{-5}$ which corresponds to a mean cosine of scattering $\bar{\mu}_0 = 0.99913$ and a mfp $\lambda = 3.38 \times 10^{-6}$ cm. This yields $\tilde{\lambda}_1/\lambda = 257$, $\tilde{\lambda}_2/\lambda = 91$, and $\tilde{\lambda}_4/\lambda = 34$, and indicates that considerable reduction in the average number of collisions per history is realizable with the moment preserving method.

3.2 Inelastic Energy-Loss

Inelastic energy-loss process and the elastic angular-scattering process share important characteristics. In particular, the large total inelastic cross section and the high probability of small energy transfers gives a GFP expansion in energy that is analogous to the angular expansion of Leakeas and Larsen [5] and is unstable or divergent when truncated beyond strictly Fokker-Planck. However, in the Fokker-Planck approximation, only the mean and mean square energy loss per unit path length traveled are incorporated. The neglect of higher order moments yields a symmetric near-Gaussian energy spectrum that is only accurate for thick targets. It was further demonstrated that just as in the approach of Leakeas and Larsen [5], the GFP expansion could be renormalized to yield a stable expansion to all orders such that energy-loss moments up to any desired order were identical to the analog values. This expansion was then reduced to an effective integral inelastic scattering operator with an explicit energy-loss kernel that was easy to sample from. Numerical results showed that preserving four energy-loss moments was sufficient to yield accurate energy spectra for

even very thin targets.

Here we further extend the analogy to elastic scattering and develop a discrete energy-loss model for inelastic interactions also. We define the energy-loss moments of the inelastic DCS by,

$$\sigma_{n,in}(\vec{r}, E) \equiv \int_0^E dE' \, (E - E')^n \sigma_{s,in}(\vec{r}, E \to E'), \quad n = 1, 2, \ldots \tag{7}$$

We then approximate the inelastic DCS by a discrete energy-loss model,

$$\tilde{\sigma}_{s,in}(\vec{r}, E') = \sum_{l=1}^{L} \frac{\beta_l(\vec{r}, E)}{2\pi} \, \delta \left[E' - \zeta_l(\vec{r}, E) \right], \tag{8}$$

where the amplitudes $\{\beta_l,\, l = 1, 2 \ldots \, L\}$ and energy-losses $\{\zeta_l,\, l = 1, 2 \ldots \, L\}$ are constrained to yield the exact first $2L$ energy-loss moments $\{\tilde{\sigma}_{l,in} = \sigma_{l,in},\, l = 1, 2 \ldots 2L\}$. All higher moments $\{\tilde{\sigma}_{l,in},\, l = L + 1, L + 2 \ldots\}$ are then expressed in terms of these lower moments. Thus, for $L = 1$ (i.e. a single discrete term) the correct stopping power and straggling coefficient are obtained. It is important to note that unlike the Fokker-Planck approximation for straggling, all higher energy-loss moments are extant in the discrete representation, albeit approximately. Moreover, the discrete model yields a strictly downscatter representation of energy loss, faithful to the analog process (the Fokker-Planck model approximates straggling as a diffusion in energy and hence includes upscatter as well.) We conclude that the discrete energy-loss model for $L = 1$ has potential accuracy exceeding that of the Fokker-Planck approximation with the same stopping power and straggling coefficient.

The parameters $\{\beta_l,\, \zeta_l\}$ in Eq.(8) are obtained by constructing an invertible linear mapping of the discrete energy-loss representation to a pseudo-elastic scattering representation similar to Eq.(6). The procedure outlined by Sloan [8] is then used to compute the parameters of the pseudo-process, and the inverse mapping gives $\{\beta_l,\, \zeta_l\}$.

Similar to the angular scattering approximation, the energy-loss mfp corresponding to L discrete energy-losses is given by $\tilde{\lambda}_L = \left(\sum_{l=1}^{L} \beta_l \right)^{-1}$ and can be used as a measure of the potential speed-up over the analog case. Again, we consider 1 MeV electrons incident on a gold target and inelastic scattering described by the Rutherford kernel [10]. The analog cross section has a mfp $\lambda = 5.84 \times 10^{-4}$ cm. This yields $\tilde{\lambda}_1/\lambda = 14.7$, $\tilde{\lambda}_2/\lambda = 6.1$, and $\tilde{\lambda}_4/\lambda = 2.8$, and indicates that less speed-up is available by approximation of energy-loss than by approximation of angular scattering. The energy-loss approximation can be expected to have more impact on calculations in low-Z materials. For 1 MeV electrons incident on water, the analog mfp is $\lambda = 8.57 \times 10^{-4}$ cm, and the ratio of mfps yields $\tilde{\lambda}_1/\lambda = 82.8$, $\tilde{\lambda}_2/\lambda = 29.7$, and $\tilde{\lambda}_4/\lambda = 11.3$.

4 Numerical Approach

The calculations presented are conducted with simplified physics both for simplicity of implementation and to isolate the effects of the algorithms being tested. No secondary photons or electrons are simulated. Angular scattering is modeled using the screened Rutherford scattering model [10]. The discrete approximation requires only cross section moments, so

the more accurate Mott cross sections [2] can be simulated also, but analog benchmarks are easier to obtain for the screened Rutherford case. The angular deflection of the primary electron due to inelastic scattering is not simulated. A common approximation is to include the effect in the angular scattering cross section moments without correlation to energy loss [10], and this could easily be included in our approach.

Inelastic interactions are also represented using a Rutherford energy loss model [10]. The moments of the more accurate Möller cross section [2] can easily be used in the discrete model, but analog benchmarks are easier to obtain for the Rutherford scattering model.

The energy dependence of the simulation is accomplished by defining all physics parameters on an energy grid. The grid is logarithmically distributed with 8 values for every halving of energy. The physical parameters used by the code are simply the angular-scattering moments and the energy-loss moments. The angular-scattering moments are computed from Eq.(5) with the screened Rutherford scattering cross section given by:

$$\sigma_{s,el}(\vec{r},\mu_0,E) = \frac{\sigma_{el,0}}{2\pi}\frac{2\eta\,(1+\eta)}{(1+2\eta-\mu_0)^2}, \tag{9}$$

where η is the screening parameter and $\sigma_{el,0}$ is the total elastic scattering cross section. The energy-loss moments are computed from Eq.(7) with the Rutherford cross section given by:

$$\sigma_{s,in}(\vec{r},E\rightarrow E') = \begin{cases} \frac{Z\rho N_A}{A}\frac{2\pi R_0^2 m_e c^2}{\beta^2 Q^2}, & Q_{min}\le Q\le \frac{E}{2} \\ 0, & \text{otherwise} \end{cases}, \tag{10}$$

where

$$\beta^2 = \frac{\tau(\tau+2)}{(\tau+1)^2}, \tag{11}$$

$$\tau = \frac{E}{m_e c^2}, \tag{12}$$

$Q = (E - E')$ is the energy loss, N_A is Avogadro's number, R_0 is the classical electron radius, m_e is the electron rest mass, c is the speed of light in vacuum, ρ is the material density, A is the average atomic weight of the material, and Z is the average atomic number of the material. For our calculations Q_{min} is chosen to be the mean excitation energy of the material. While this is a somewhat arbitrary choice, it gives reasonable results. A more accurate choice could be obtained by matching appropriate low-order energy-loss moments to experimental values, but this is beyond the scope of the present investigation. In the calculations discussed here, the cutoff energy is set at one percent of the source energy or at two times the mean excitation energy, whichever is greater.

In the continuous slowing down (CSD) approximation, only the first moment of energy-loss, the mean energy-loss per unit distance, is retained. That is, all higher order energy-loss moments are neglected, so that in the absence of elastic scattering an electron will always lose the same amount of energy in travelling a fixed distance. In implementation, we assume that the mean energy-loss is piecewise constant based on the grid point nearest in energy.

Our implementation of the condensed history method is based on sampling from Goudsmit-Saunderson distributions divided into 33 non-uniform angular bins. The method we label

as "ITS-like Condensed History" (or "ITS-like CH") applies the multiple-scattering angular deflection of the particle at the end of each step, i.e. the end of the pathlength for which the angular deflection has been precomputed. The algorithm differs from the strict implementation in the ITS codes in that: our angular distribution is based on the simpler screened Rutherford scattering and ignores angular deflection due to inelastic scattering; we sample from the precomputed angular deflection distribution nearest in energy to the energy of the particle when the angular deflection is applied; we have implemented a simpler material boundary crossing algorithm; and we use the CSD approximation. These modifications simplify the implementation and seem reasonable for arriving at a consistent basis for comparison with other methods. The same simplifications apply to the "Random Hinge Condensed History" (or "Random Hinge CH") algorithm. It differs from the ITS-like algorithm only in that the angular deflection of the particle is applied at a uniformly sampled random position within each step.

The discrete angle and discrete energy scattering parameters (α_l, ξ_l, β_l, and ζ_l) are precalculated on the energy grid. The electron transport code uses these parameters based on the nearest grid point to the energy of the particle. This energy grid has been found to be sufficiently refined to yield accurate results. Efficiency improvements may be achieved by coarsening this grid, possibly while using a more sophicated interpolation method. For the condensed history schemes, the angular distributions of the nearest grid point are used. The Goudsmit-Saunderson angular distributions are stored in 33 angular bins as a cumulative probability function for ease of sampling during the calculation. For analog calculations, parameters used in sampling scattering directions are also precomputed to make the Monte Carlo calculation computationally efficient. While most of the results shown are one dimensional, Monte Carlo tracking is performed in all three spatial dimensions for all methods.

While the computer code in which these methods have been implemented has been written to be efficient for all methods and to provide a fair efficiency comparison between the methods, it is important to note that independent efficiency improvements may be possible in the algorithms employed for each of the methods. Some variation in relative runtimes could also be expected on different computer architectures. Runtime comparisons should be considered approximate due to these uncertainties.

5 Depth-Dose Profiles

In this section we present one-dimensional results from three sets of calculations with two types of problems. The results are based on calculating the transversely-integrated dose in layers within the slabs of materials. We examine the angular approximations (with CSD in energy), the energy approximations (with analog angular-scattering), and the combined discrete angular-scattering and energy-loss approximations.

For each of these three sets of calculations, we first illustrate that this method can generate accurate results in a regime of relatively isotropic scattering. This is a regime in which traditional condensed history transport methods have some difficulty. Specifically, we simulate 250 keV electrons incident on a 0.008 cm thick slab of gold.

Next, we illustrate that this method can generate accurate results in a regime of highly forward-peaked scattering by considering 20 MeV electrons incident on a 30 cm thick slab

of water. This is a regime in which traditional condensed history transport methods perform quite well. It is also a regime in which energy-losltiple-scattering approximations of condensed history algorithms. All of the calculations in this section use continuous slowing down (CSD) in energy, so the effects of the angular approximations may be isolated. Within this section the term "Analog" refers to the analog simulation of angular scattering and CSD in energy. These analog results are the benchmarks against which other calculations are compared for accuracy.

The transversely-integrated dose for 250 keV electrons incident on gold is shown in Fig. 1. Only results that have observable differences from the analog results are shown here. The lower panel of the figure shows the statistical uncertainty of the analog results as a percent of the dose. Note that at large depths the dose levels are not observable on a linear scale and have large statistical uncertainties. The relative error of the methods as compared with the analog benchmark is shown in Fig. **??**. The lower panel of the figure shows the statistical uncertainty of the relative error of the 4 Discrete Angles results in the same unitless dimension. At depths beyond 0.005 cm, the statistical uncertainty is large enough to obscure any real differences in the dose values.

In these and following figures, the statistical uncertainty is plotted for only one of the results in each figure, so as to improve the clarity of the figure. The uncertainties of other results were observed to have approximately the same magnitudes and to exhibit the same trends as a function of depth. This is almost always the case, with a single exception among our results. Dose calculations with CSD in energy are found to have different statistical uncertainties than results using other energy-loss approximations. This difference can be observed by comparing the statistical uncertainty in the plots of angular-scattering approximations in this section (all using CSD) and the plots of energy-loss approximations in the following section (where the statistical uncertainty plots are not based on CSD).

In both Figs. 1 and **??** the inaccuracies of the "ITS-like CH" approximation are clearly evident. The ITS-like approximation, by imposing the angular deflection at the end of each condensed history step, assumes that the angular deflection of the particle is generally very forward-peaked. These results demonstrate that the forward-peaked assumption is inadequate at low electron energies in high-Z materials. It underestimates the dose at shallow depths and over-estimates the dose through the remainder of the dose profile. In the plot of relative error, we observe that the 1 Discrete Angle approximation oscillates mildly about the analog results at shallow depths. Small but statistically-significant differences of the 2 Discrete Angles and Random Hinge approximations can be seen also. However, both are generally within 1 percent of the analog results, which is likely to be deemed a practically-insignificant difference given the uncertainties in realistic cross section models.

The transversely-integrated dose for 20 MeV electrons incident on water is shown in Fig. **??**, and the relative error of the methods is shown in Fig. 2. Only the 1 Discrete Angle approximation has visible inaccuracies in this problem, but the relative error remains less than 4% except at large depths. The 2 Discrete Angles approximation can be observed to oscillate about the analog result with errors of less than 1% except at large depths.

While we must be primarily concerned with obtaining accurate results, a secondary concern of great importance is the speed with which the calculations can be performed. As previously mentioned there are many sources of variation in the measure of computational speed, but it is informative to state the speed-up that we observed relative to analog cal-

culations. These speed-ups are given in Table 1. We include the speed-ups for the results we have presented, as well as for two intermediate problems. Not surprisingly, the speed-up of the discrete scattering-angle approximations scales roughly by the mean free paths as suggested in Section 3.1. Note that the speed-ups given here for 1 MeV electrons on gold are not as large as predicted from the cross sections, because these speed-ups are based on energy-dependent calculations and the speed-up decreases with decreasing electron energy. The 1 Discrete Angle approximation gives by far the largest speed-up in all cases. Thus, we note that even this approximation that is generally less accurate may nevertheless be deemed to be accurate enough for fast scoping calculations.

The condensed history methods, using step-sizes based on the ITS implementation of the method, gives speed-ups that are generally on the same order of magnitude as the 2 Discrete Angles approximation. Some implementations of the condensed history method allow variation of the step-size, thus varying the speed of the calculations. Altering the step-size could be expected to have some effect on the accuracy of the method as well. We have not performed such an analysis but merely note that the step-sizes in the ITS implementation have been extensively studied and carefully selected.

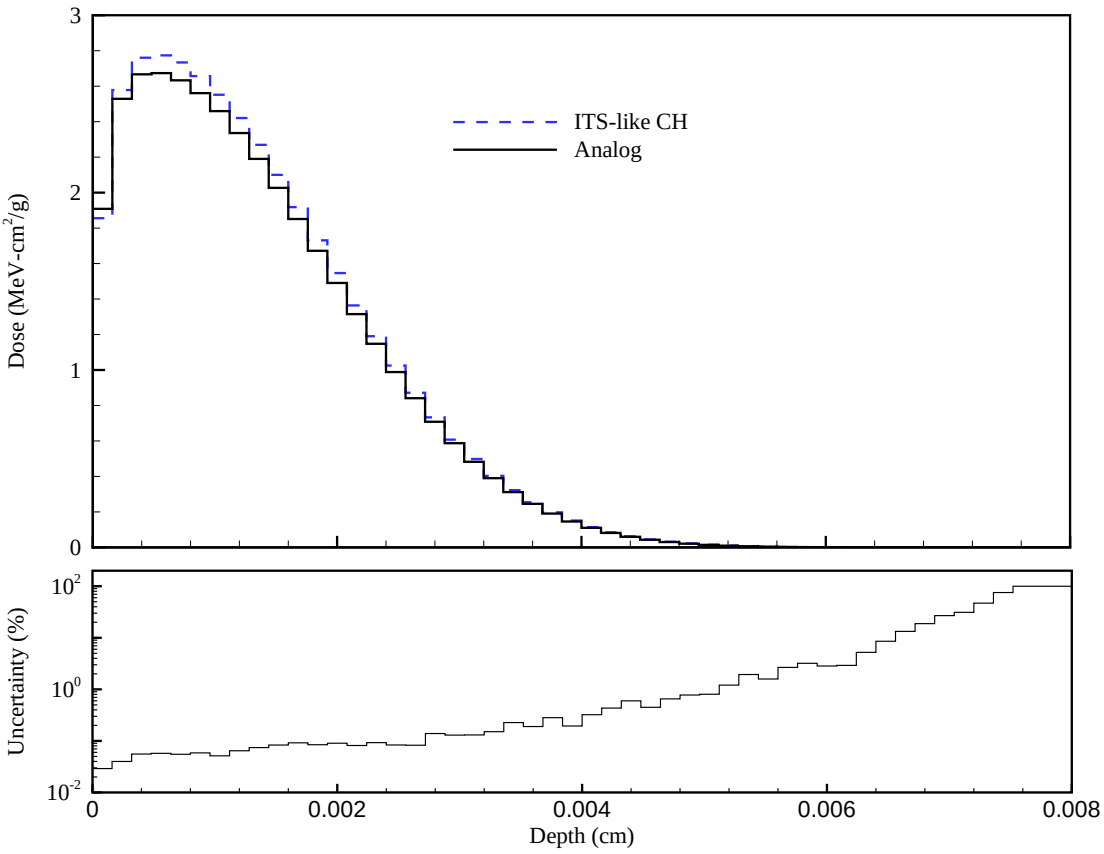

Figure 1: **Dose from 250 keV electrons on gold with angular-scattering approximations and the associated statistical uncertainty.**

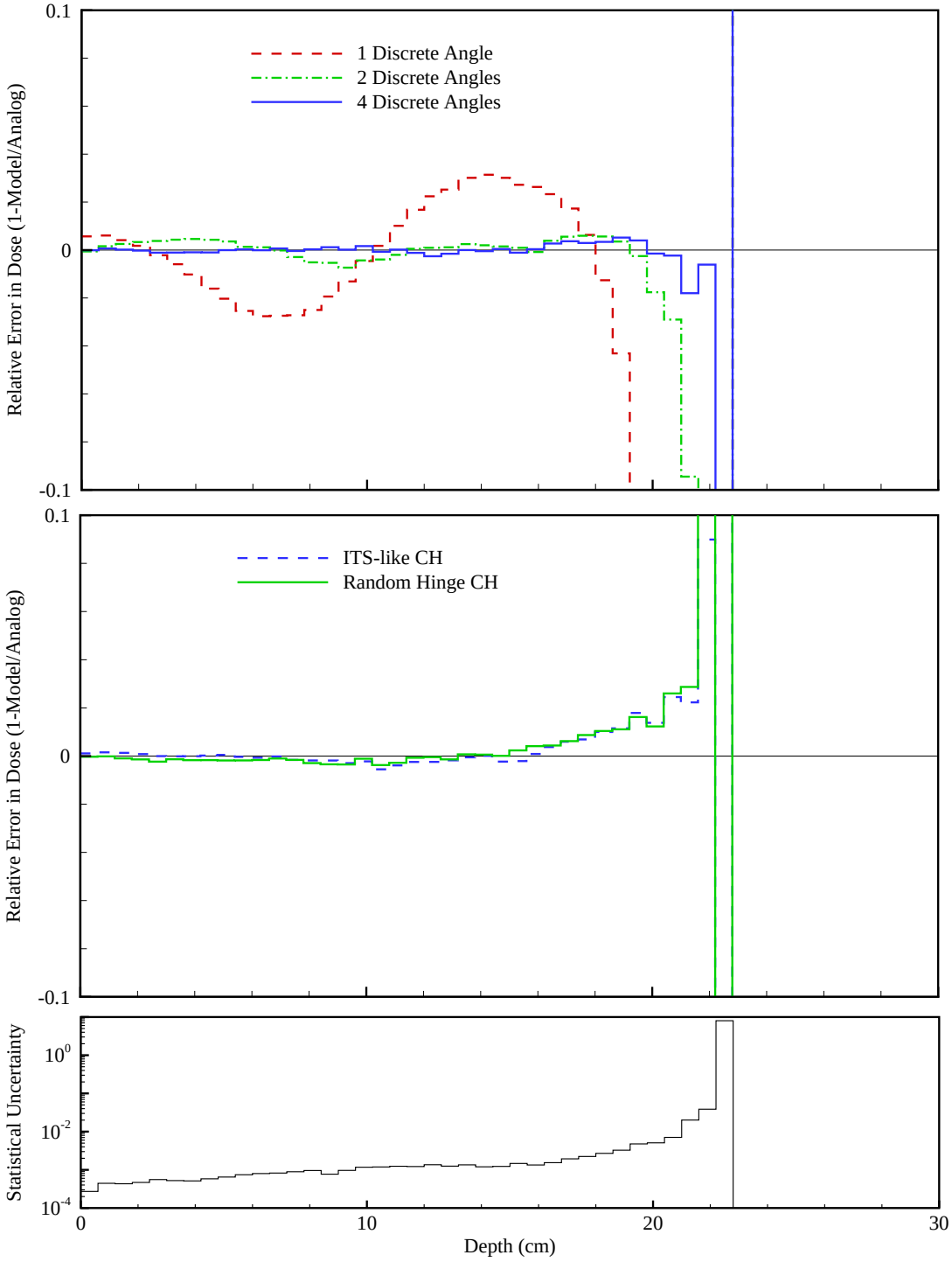

Figure 2: **The relative error (in dose from 20 MeV electrons on water) of approximate angular-scattering models compared with analog Monte Carlo results and the associated statistical uncertainty.**

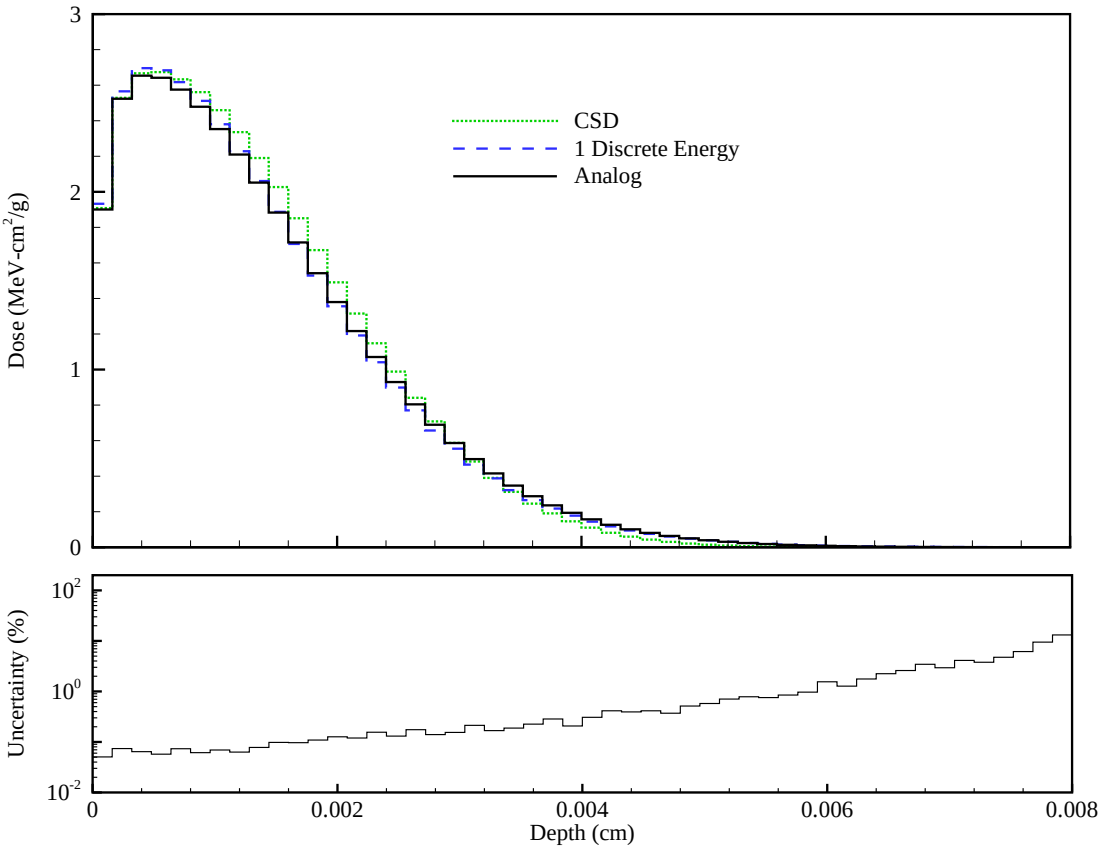

Figure 3: **Dose from 250 keV electrons on gold with energy-loss approximations and the associated statistical uncertainty.**

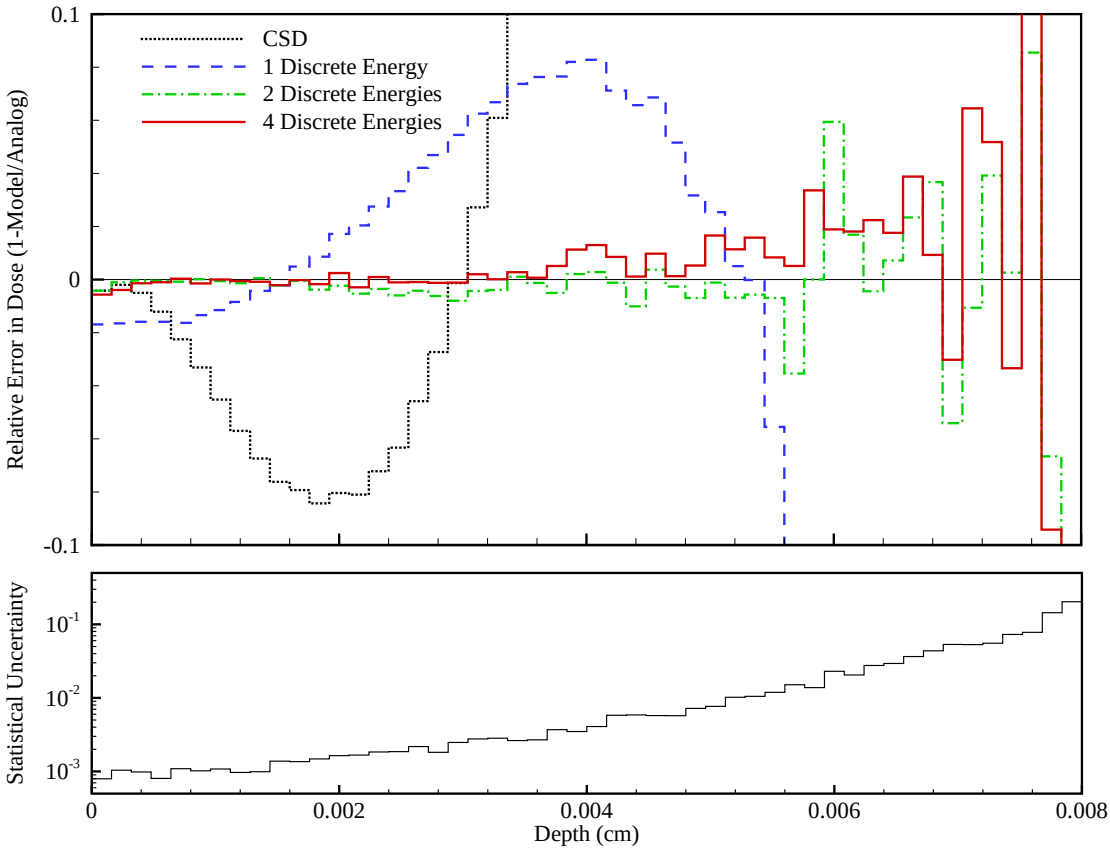

Figure 4: **The relative error (in dose from 250 keV electrons on gold) of approximate energy-loss models compared with analog Monte Carlo results and the associated statistical uncertainty.**

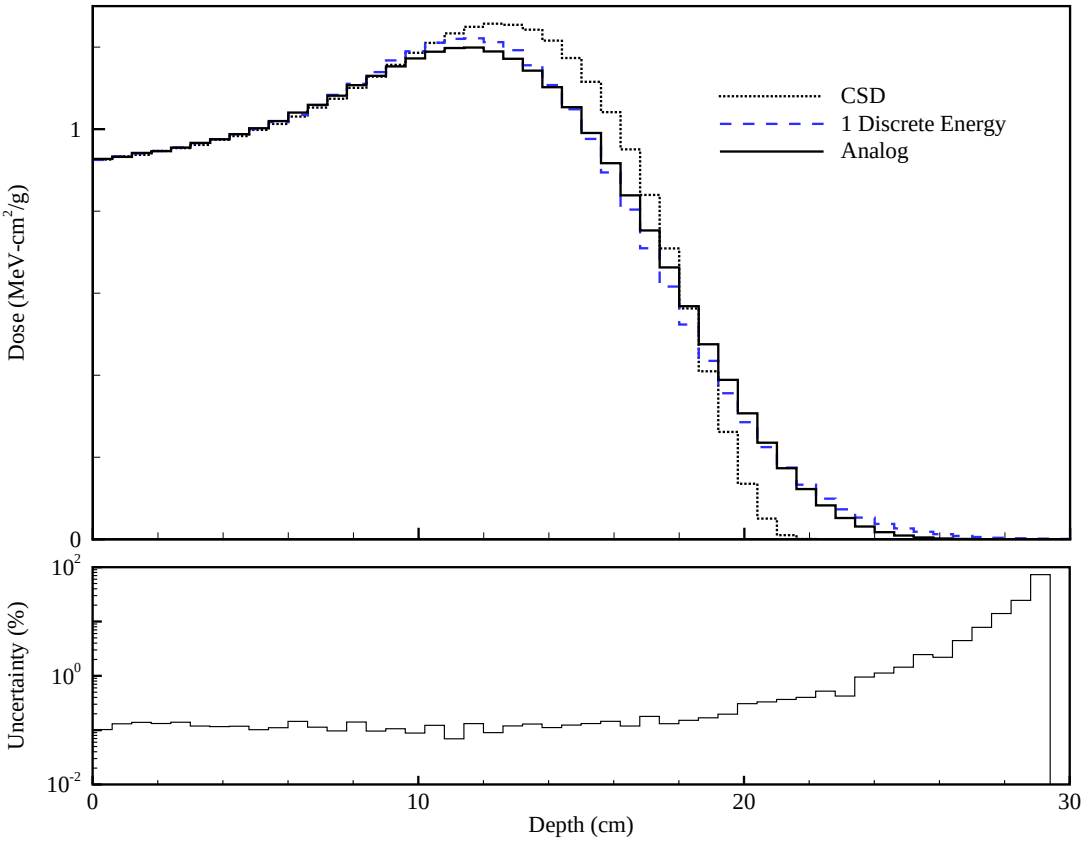

Figure 5: **Dose from 20 MeV electrons on water with energy-loss approximations and the associated statistical uncertainty.**

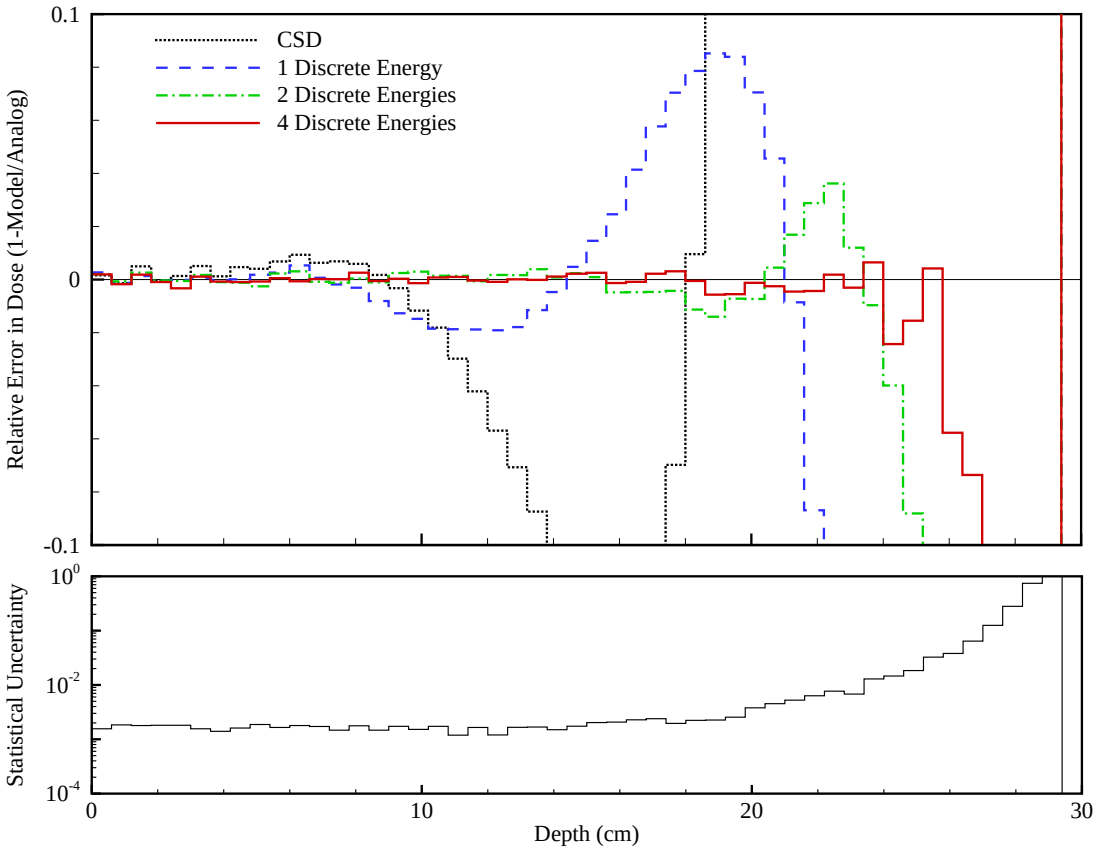

Figure 6: **The relative error (in dose from 20 MeV electrons on water) of approximate energy-loss models compared with analog Monte Carlo results and the associated statistical uncertainty.**

Table 1: **Speed-up of Approximate Angular-Scattering Methods Over Analog Monte Carlo with CSD in Energy.**

Scattering-Angle Approximation	Speed-up Factor			
	20 MeV on H_2O	1 MeV on H_2O	1 MeV on Au	250 keV on Au
1 Angle	1973.4	143.0	62.7	17.6
2 Angles	947.2	65.1	26.2	8.5
4 Angles	392.0	28.5	11.8	4.6
ITS-like CH	555.6	47.4	34.1	8.8
Random Hinge CH	493.9	42.6	30.8	8.1

6 Implementation of Moment-Preserving Straggling Model in MCNP

We now describe and demonstrate an improved condensed history (CH) [1] electron energy-loss straggling model by implementing it directly in MCNP. In most CH implementations [11, 15, 14], electron energy losses are sampled from the Landau distribution [1, 17] which is an approximate solution to the transport equation, ignoring deflection and valid for thin slabs. Although the model is accurate under such conditions, it is difficult to refine for enhanced accuracy and to apply under more general circumstances. Here we propose a different method for accurately computing the straggling distribution, based on simulating the electron energy loss through each step by single event Monte Carlo in conjunction with a simplified energy-loss cross section. This new straggling model and algorithm has been implemented and tested in MCNP and shown to be potentially more accurate than the traditional method reliant on sampling the Landau distribution. In the ensuing we present the methodology along with demonstrative numerical results.

6.1 Electron Energy-Loss Straggling

In the CH method, straggling distributions are ideally given by solutions to the following transport equation without deflection,

$$\frac{\partial \psi(s,E)}{\partial s} = \int_{Q_{min}}^{Q_{max}} \Sigma_{e^-}(E+Q,Q)\psi(s,E+Q)\,\mathrm{d}Q - \Sigma_{e^-}(E)\psi(s,E), \tag{13}$$

where $\psi(s,E)$ is the flux as a function of pathlength s and energy E, $\Sigma_{e^-}(E)$ is the total cross section, $\Sigma_{e^-}(E+Q,Q)$ is the differential cross section for energy loss Q in a collision which is often approximated by the Rutherford cross section but is more accurately given by the Moller formula [10]. The maximum energy transfer possible Q_{max} is given by the collision kinematics, accounting for the indistinguishability of incident and recoiling electrons [**?**]. The minimum energy Q_{min} is set equal to the mean ionization energy of the target atom so that our investigations are restricted to hard collisions only. The incorporation of mean and mean-square energy losses associated with soft (sub-ionization threshold) collisions is quite straightforward in our method and depends only on the availability of relevant models or data for these moments.

The Landau distribution [17] represents a solution to Eq.(13) subject to two important approximations. First, the mean free path of the electron is held constant throughout the step, amounting to fixing E at its initial value, and second, Q_{max} is allowed to become unbounded. Both approximations were introduced to facilitate analytic solution of Eq.(13) using a Laplace transform in the energy variable. The subsequent inverse transform, while not explicitly possible, was simplified enough to be numerically evaluated and stored for sampling. The first approximation requires the mean energy loss to be small compared to the incident electron energy, while the second is justified on the grounds that the differential cross section for large energy transfers varies as $\sim 1/Q^2$ and hence relaxing the upper bound should not measurably affect the result. While the former approximation is reasonable for sufficiently thin layers or small step sizes, the second, however, results in the Landau

distribution yielding an unbounded mean energy loss. This then necessitates the application of an artificial cut-off in the spectrum so as to keep the mean energy loss finite. We next briefly describe our alternative approach which does not require the above approximations.

6.2 Moment Preserving Cross Sections

Key to our approach is the accurate and inexpensive solution of the straggling equation given by Eq.(13) over a step length. This is clearly not feasible when the true or analog differential cross section is employed but we have already demonstrated that modeled differential cross sections that preserve a finite number of energy-loss moments are capable of yielding accurate representations of energy spectra and dose. We recall that the energy-loss moments of the analog cross section are defined by,

$$Q_n = \int_{Q_{min}}^{Q_{max}} \mathrm{d}Q\, Q^n \Sigma_{e^-}(E, Q), \quad n = 1, 2 \ldots . \tag{14}$$

No attempt is made to preserve the true mean free path but it has been demonstrated that if lower order moments of the true cross section, such as the mean and mean-square energy losses which capture the bulk of the dominating small energy transfers, are rigorously preserved while higher order moments, describing less frequent larger energy transfers, are reasonably accurately approximated, the resulting modeled cross section tends to be considerably smoother and the mean free path considerably longer [18, 16, 19]. This greatly facilitates the numerical solution of Eq.(13) by any method and by Monte Carlo in particular, as we demonstrate below.

Clearly, there is no unique method for constructing moment-preserving approximations to the analog cross section, but we have identified two formulations that work extremely well. In one, we use a cross section representation that preserves a preset number of energy-loss moments through a superpostion of discrete energy losses. While a purely discrete cross section representation is ideal for sampling energy losses in Monte Carlo, not surprisingly discrete artifacts arise and, indeed, can dominate the straggling distribution. To mitigate these artifacts, we supplement the discrete representation with a continuous-in-energy component in our second approach, to create a hybrid discrete-continuous cross section. Specifically, we use the exact Möller differential cross section to describe large energy transfer collisions and a discrete component to ensure lower moments are preserved. An interpolating parameter is introduced to connect the two components. The following sections describe, in detail, the purely discrete and hybrid energy-loss models.

6.2.1 Purely Discrete Energy-Loss Model

The purely discrete scattering distribution was originally used to approximate elastic scattering. In this setting, the approximate differential cross section can be represented as a superposition of discrete scattering angles as

$$\Sigma^*_{el}(E, \mu_0) = \sum_{l=1}^{L} \frac{\gamma_l(E)}{2\pi} \delta[\mu_0 - \xi_l(E)], \tag{15}$$

where $\Sigma_{el}(E, \mu_0)$ is the approximate elastic scattering cross section for a particle with incident scattering cosine μ_0, and incident energy E. In Eq.(15), ξ_l are the discrete scattering cosines with their corresponding amplitudes γ_l, for $l = 1, 2 \ldots L$. The scattering angles and amplitudes are constrained to exactly yield the first $2L$ momentum transfer moments of the analog differential elastic scattering cross section, given by

$$\Sigma_{n,el,mom}(E) = 2\pi \int_{-1}^{1} \mathrm{d}\mu_0 (1 - \mu_0)^n \Sigma_{el}(E, \mu_0),\ n = 1, 2 \ldots . \tag{16}$$

Due to the similarities in the cross sections (i.e. steep cross sections for decreasing energies and steep cross sections for small angle scatters), it is possible to extend the idea of a discrete distribution to represent the continuous angular distribution to a discrete energy-loss distribution. With this we can represent the differential energy-loss cross section as a superposition of discrete energy-losses,

$$\Sigma^*_{e^-}(E, Q) = \sum_{l=1}^{L} \alpha_l \delta[Q - \overline{Q}_l]. \tag{17}$$

In Eq.(17), we have $\overline{Q}_l$ discrete energy losses and the corresponding weights α_l, for $l = 1, 2 \ldots L$. As with the discrete angular distribution, these discrete energy-losses and weights give $2L$ free parameters with which we can preserve exactly $2L$ energy-loss moments. The advantage of this approximate cross section is that we now have a systematic method of preserving energy-loss moments to a desired order. For every discrete energy-loss we add to the distribution, we preserve two additional energy-loss moments.

Preserving the moments requires that we set the energy-loss moments of Eq.(17) to the exact energy-loss moments. For example, if we use $L = 1$ so that we preserve the first two energy loss moments, we form the following non-linear system of algebraic equations,

$$\begin{aligned} Q_1 &= \alpha_1 \overline{Q}_1, \\ Q_2 &= \alpha_1 \overline{Q}_1^2, \end{aligned} \tag{18}$$

where Q_1 and Q_2 are the exact moments of the Möller differential energy-loss cross section. Using substitution, the system can be solved for α_1 and $\overline{Q}_1$ in terms of Q_1 and Q_2,

$$\overline{Q}_1 = \frac{Q_2}{Q_1}, \tag{19}$$

$$\alpha_1 = \frac{Q_1^2}{Q_2}. \tag{20}$$

Because we set the first and second moments of Eq.(17) to the exact moments of the appropriate energy-loss distribution, we are exactly preserving the first two energy-loss moments of the total cross section. However, by only preserving these two low order moments, we are essentially approximating the total cross section and all higher order moments by Q_1 and Q_2.

6.2.2 Higher Order Approximations

For higher order approximations (i.e., $L > 1$), there is no simple analytic solution for the non-linear system of equations. It is possible that one could solve the system using a Newton iteration scheme, but convergence is observed to be very slow. Sloan [8] reworked an algorithm in the code MORSE [7] to calculate discrete angles and corresponding weights using a Radau quadrature. The original MORSE implementation used a gauss quadrature to produce angles and weights, preserving the Legendre moments of the angular scattering distribution. The refined method uses the Legendre coefficients, given by the Legendre moments of the elastic cross section,

$$\Sigma_{l,el,leg}(E) = 2\pi \int_{-1}^{1} \mathrm{d}\mu_0 P_l(\mu_0)\Sigma_{el}(E,\mu_0),\ l = 1, 2\ldots, \tag{21}$$

where $P_l(\mu_0)$ are the Legendre polynomials of μ_0. The Legendre coefficients are given by,

$$f_l = \frac{\Sigma_{l+1,el,leg}}{\Sigma_{0,el,leg}},\ l = 0, 1, 2\ldots. \tag{22}$$

Sloan's revision to the MORSE algorithm uses the calculated Legendre coefficients and first calculates Gauss moments, and using differences between successive Gauss moments, Radau moments are generated. The algorithm preserves the total cross section and $2L$ moments in $L + 1$ angles, where the forward angle, $\mu_0 = 1$, is always preserved. Using the Radau quadrature solution, the distribution can now be represented as

$$\Sigma^*_{el}(E,\mu_0) = \frac{\gamma_0}{2\pi}\delta[\mu_0 - 1] + \sum_{l=1}^{L} \frac{\gamma_l(E)}{2\pi}\delta[\mu_0 - \xi_l(E)],\ l = 1, 2\ldots, \tag{23}$$

where the forward direction $\mu_0 = 1$ represents a collision in which no scattering occurs at all. Knowing this we can essentially eliminate the delta function for the forward direction from Eq.(23), to get

$$\Sigma^*_{el}(E,\mu_0) = \sum_{l=1}^{L} \frac{\gamma_l(E)}{2\pi}\delta[\mu_0 - \xi_l(E)], \tag{24}$$

and we can now calculate the corresponding total cross section as

$$\Sigma^*_{el}(E) = \left(\sum_{l=1}^{L} \gamma_l\right) - \gamma_0, \tag{25}$$

where $\Sigma^*_{el}(E)$ is now reduced by the weight of the forward direction, and thus gives a reduction in the total cross section and an increase in the mean free path. In other words, the use of the forward angle has preserved the higher order moments of the distribution, and yielded a system with a cross section that is smaller in magnitude and less forward peaked than the analog cross section.

6.2.3 Linear Mapping from Energy to Angle

The underlying similarities between elastic and inelastic scattering cross sections lead to using the algorithm developed by Sloan as a method to solve for $\overline{Q}_l$ and α_l from Eq.(17). As mentioned previously, this algorithm uses the Legendre coefficients of the elastic scattering differential cross section.

Given an energy-loss cross section (i.e., the Möller), we wish to map the cross section $\Sigma_{e^-}(E,Q)$, $0 < Q < Q_{max}$, to a pseudo-scattering cross section $\widetilde{\Sigma}(E,\mu_0)$, for $-1 < \mu_0 < 1$. Here, μ_0 is the directional cosine of the pseudo-scattering angle, and we constrain $\widetilde{\Sigma}(E,\mu_0)$ so that the momentum transfer moments, $\Sigma_{l,el,mom}$, or the Legendre moments, $\Sigma_{l,el,leg}$ can be related directly to the energy-loss moments (Eq.(14)). This constraint is achieved by assuming a one-to-one relationship between μ_0 and Q, so that we have

$$2\pi\widetilde{\Sigma}(E,\mu_0)\mathrm{d}\mu_0 = \Sigma_{e^-}(E,Q)\mathrm{d}Q. \tag{26}$$

If we further assume that we have a known invertible mapping, i.e.,

$$Q = T(\mu_0), \tag{27}$$
$$\mu_0 = T^{-1}(Q), \tag{28}$$

we can obtain an explicit pseudo-scattering cross section from using the energy-loss cross section, given by

$$\widetilde{\Sigma}(E,\mu_0) = \frac{1}{2\pi}\Sigma[T(\mu_0)]\left|\frac{\mathrm{d}T}{\mathrm{d}\mu_0}\right|. \tag{29}$$

Because we have assumed a one-to-one relationship, we can form the linear mapping of the form

$$Q = T(\mu_0) = a + b\mu_0, \tag{30}$$

where a and b are selected such that $T(1) = 0$ and $T(-1) = Q_{max}$, i.e., a forward scatter corresponds to zero energy-loss and a backscatter corresponds with a maximum energy-loss. Using these conditions, we find

$$0 = a + b, \tag{31}$$
$$Q_{max} = a - b, \tag{32}$$

yielding the following

$$a = \frac{Q_{max}}{2}, \tag{33}$$
$$b = -\frac{Q_{max}}{2}. \tag{34}$$

Using the results for a and b, we now have an explicit mapping

$$Q = T(\mu_0) = \frac{Q_{max}}{2}(1-\mu_0), \tag{35}$$

and it's inverse

$$\mu_0 = T^{-1}(Q) = 1 - \frac{2Q}{Q_{max}}. \tag{36}$$

In the case that the cross section for $Q < Q_{min}$ is not defined, we set $\Sigma(E, Q) = 0$ for $0 \leq Q < Q_{min}$, giving us a cutoff value for μ_0 of

$$\mu_{cut} = 1 - \frac{2Q_{min}}{Q_{max}}, \tag{37}$$

in turn giving an analogous condition on the pseudo-scattering cross of $\widetilde{\Sigma}(E, \mu_0) = 0$ for $-1 \leq \mu_0 < \mu_{cut}$.

With these relationships, we can now directly calculate either the Legendre or momentum-transfer moments of the pseudo-scattering cross section directly, and obtain the Legendre coefficients necessary for refined MORSE algorithm to create pseudo-scattering angles and their corresponding weights.

We also present an alternative method for finding the Legendre coefficients using a direct relationship between the energy-loss moments of the inelastic scattering cross section and the momentum transfer moments of the pseudo-scattering cross section (using the linear mapping from energy to angle). With the momentum transfer moments of the pseudo-scattering cross section, we can form a direct relationship between the momentum transfer moments and the energy loss moments. Manipulating Eq.(35) we obtain the following relationship between Q and $(1 - \mu_0)$

$$1 - \mu_0 = \frac{2Q}{Q_{max}}. \tag{38}$$

Using Eq.(38) in Eq.(16), we can now represent the momentum transfer moments directly in terms of the energy-loss moments:

$$\widetilde{\Sigma}_{l,el,mom} = \left(\frac{2}{Q_{max}}\right)^l \int_{Q_{min}}^{Q_{max}} Q^l \Sigma_{e^-}(E, Q), \tag{39}$$

where we can see that the integral in Eq.(39) is exactly equivalent to Eq.(14). The direct relationship between the energy-loss moments and the momentum transfer moments is then given by

$$\widetilde{\Sigma}_{l,el,mom}(E) = \left(\frac{2}{Q_{max}}\right)^l Q_l, \tag{40}$$

where Q_l are the energy-loss moments. To obtain the Legendre coefficients, however, we must now relate the momentum transfer moments to the Legendre moments. To do this, we first perform a Taylor series expansion of $P(\mu_0)$ about $(1 - \mu_0)$, which is shown as

$$P_l(\mu_0) = P_l(1 - (1 - \mu_0)) = \sum_{n=0}^{l} c_n \frac{(-1)^n}{n!}(1 - \mu_0)^n, \tag{41}$$

where c_n are dependent on the Legendre polynomials [**?**], and given as

$$c_n^l = \frac{\mathrm{d}^n}{\mathrm{d}{\mu_0}^n} P_l(\mu_0)\bigg|_{\mu_0=1}. \tag{42}$$

The Taylor series expansion in Eq.(41) truncates at $n = l$ due to the fact that P_l is a polynomial of degree l and only has a maximum of l nonzero derivatives. The recursion relationship for c_n^l [**?**] is given by

$$c_n^l = \frac{1}{2^n n!} \prod_{i=0}^{n-1} \big[l(l+1) - i(i+1) \big]. \tag{43}$$

Using the pseudo-scattering cross section and Eq.(41) in Eq.(21), we obtain

$$\widetilde{\Sigma}_{l,el,leg}(E) = \sum_{n=0}^{l} c_n^l 2\pi \int_{-1}^{1} \mathrm{d}\mu_0 (1-\mu_0)^n \widetilde{\Sigma}(E, \mu_0), \tag{44}$$

where the integral on the right hand side of the equation is equivalent to the momentum transfer moments given by Eq.(16), so we can now represent the Legendre moments of the pseudo-scattering cross section in terms of the momentum transfer cross section:

$$\widetilde{\Sigma}_{l,el,leg}(E) = \sum_{n=0}^{l} c_n^l \widetilde{\Sigma}_{n,el,mom}(E). \tag{45}$$

With Eq.(40), we now can represent the Legendre moments in terms of the exact energy-loss moments (Q_n) of the appropriate differential energy-loss cross section as

$$\widetilde{\Sigma}_{l,el,leg}(E) = \sum_{n=0}^{l} c_n^l \left(\frac{2}{Q_{max}} \right)^n Q_n. \tag{46}$$

We can further simplify $\widetilde{\Sigma}_{l,el,leg}(E)$, due to the fact that for all n at $l = 0$ we have $c_n^0 = 1$, and for all $n = 0$ for $l = 1, 2 \ldots$, $c_0^l = 0$, we can write Eq.(46) in terms of the reduced total cross section, given by

$$\widetilde{\Sigma}_{l,el,leg}(E) = Q_0 + \sum_{n=1}^{l} c_n^l \left(\frac{2}{Q_{max}} \right)^n Q_n \tag{47}$$

Using the refined scattering algorithm from MORSE, the discrete scattering angles and their corresponding weights can now be calculated. From these discrete angles we can use the prescribed mapping (i.e., Eq.(30)) to map from the pseudo-scattering angle back to energy to obtain our discrete energies, $\overline{Q}_l$. These discrete energies will be comprised of $\overline{Q}_0 = Q_{min}$, and $\overline{Q}_l$ for $l = 1, 2 \ldots L$, preserving $2L$ moments of the energy-loss cross section. The weights, γ_l, are obtained from the original relationship for $\widetilde{\Sigma}(E, \mu_0)$ in Eq.(29). Using our discrete cross sections for energy-loss (Eq.(17)) and angle (Eq.(15)) in Eq.(29), we find that $\alpha_l = \gamma_l$, for all l.

It is important to note that with Eq.(46), it is no longer necessary to have an explicit differential energy-loss cross section. Although this feature of the linear mapping is not discussed in this paper, if the energy-loss moments are known (either experimentally or empirically derived energy-loss moments) it would be possible to calculate the Legendre coefficients necessary to generate a discrete energy-loss distribution.

6.2.4 Hybrid Discrete-Continuous Energy-Loss Model

The motivating factor with this model completely lies with the fact that high energy-loss collisions only occur a small fraction of time compared to low energy-loss collisions. If we represent the limiting factor of the distribution (i.e., low energy-loss collisions) by an efficient distribution (i.e., a discrete distribution) and represent the large energy-losses exactly, we can effectively smooth any artifacts caused by the discrete distribution. Discrete collisions can be smoothed if there are large numbers of collisions that occur before the quantity of interest is calculated (i.e., energy-loss spectra or dose). With energy-loss spectra, especially for thin slabs, there are large numbers of small energy-loss collisions, but for the larger energy-loss collisions there are not enough collisions that could smooth a purely discrete distribution. If we represent only the small energy-losses by the discrete energy-loss distribution, it is possible that the large number of collisions of these small energy-loss will smooth out the discrete distribution in this portion of energy-loss spectra. In addition, representing the larger energy losses by the analog cross section will of course yield exact results for higher energy transfers.

The decomposition of the distribution, so that we use a discrete cross section to represent the low energy losses by a discrete distribution and the high energy losses by the continuous analog distribution, is performed by creating a cutoff or interpolating parameter, Q^*. With Q^* we now have our hybrid cross section, given by

$$\Sigma_{e^-}(E,Q)\mathrm{d}Q = \begin{cases} \Sigma^*_{e^-}(E,Q)\mathrm{d}Q & , \quad Q_{min} \leq Q \leq Q^* \\ \Sigma_{e^-}(E,Q)\mathrm{d}Q & , \quad Q^* < Q \leq Q_{max} \end{cases} \tag{48}$$

It is highly desirable that the Q^* is chosen so that it not only represents enough of the low energy-losses so that the total mean free path from the hybrid total cross section will be reduced significantly, but still retain enough of the high energy-loss portion of the cross section so that there are no discrete artifacts due to the discrete distribution. Here we propose a method of determining Q^*, such that we preserve the mean free path of the distribution for $Q^* \leq Q \leq Q_{max}$. This gives us the following equation from which we can solve for Q^*,

$$\frac{1}{\lambda} = \int_{Q^*}^{Q_{max}} \Sigma_{e^-}(E,Q)\mathrm{d}Q, \tag{49}$$

where λ is the mean free path of the high energy-loss portion of the distribution which can be represented in terms of the total energy-loss cross section,

$$\Sigma_{e^-}(E) = \frac{1}{\lambda}. \tag{50}$$

From Eq.(49), we can now choose an arbitrary value for the mean free path, and in essence "dial" the mean free path. This is a very attractive feature of our hybrid method, as the mean free path of our distribution for $Q > Q^*$ will determine how much of the distribution will be represented by the discrete distribution. The arbitrary choice does pose a difficulty, in that we must choose the total cross section for $Q > Q^*$ so that it is large enough so that it will represent enough large energy-loss collisions exactly in turn removing any discrete artifacts from the energy-loss distribution, and also make sure that the total cross section is

small enough that we significantly reduce the total cross section of the entire distribution. It is also important to note that because we have the freedom of choosing the mean free path of the continuous portion of the cross section, as Q^* approaches Q_{min}, the total mean free path of the entire distribution approaches the analog mean free path.

To provide a systematic method in which we can calculate Q^*, we preserve the mean free path for $Q > Q*$ as one condensed history "step size". Preserving the mean free path as a step size now gives us the following relationship for Q^*,

$$\frac{1}{\lambda_{CH}} = \int_{Q^*}^{Q_{max}} \Sigma_{e^-}(E, Q)\mathrm{d}Q, \tag{51}$$

where λ_{CH} is the condensed history step size. Using the Möller differential cross section we can now calculate Q^*.

6.3 Implementation in MCNP

We have implemented our new straggling model in MCNP using the following algorithm that avoids the need for a precomputed spectrum. The electron is transported through the step using a single event Monte Carlo simulation based on the moment-preserving model cross sections described above, and the exiting energy is taken to be the incident energy for the next step. This is done for each history for successive steps until the electron is terminated. Since our approach solves the exact transport equation (without deflection), the exiting energy represents a valid sample from the exact energy distribution at the end of the step. That is, the statistically converged (with respect to the number of electron histories) straggling distribution obtained using this method constitutes a solution of Eq.(13) with the approximate cross section. Although not as fast as sampling a precomputed distribution, the use of smooth cross sections with associated mean free paths that are long compared to analog but sufficiently short compared to a step size, ensures that the Monte Carlo solution does not incur an excessive additional computational cost.

In our modification of MCNP, an option in the MCNP input deck allows for the use of either the Landau straggling model or the above moment-preserving model thereby facilitating a direct comparison of the two approaches. We note that for these comparisons to be meaningful it is necessary to ensure that the sole free parameter in the Landau distribution, namely the mean energy loss, or stopping power, is identical to that used in the new model. In generating numerical results, we have used the stopping power from the Möller cross section in both implementations. We have also implemented a third option, namely the solution of the analog problem using the same single event Monte Carlo logic as for the modeled cross section. This provides a means of benchmarking the two approximate straggling methods as well as a measure of computational efficiency realized with these methods. Finally, we mention that the angular deflections are described using the existing Goudsmidt-Saunderson multiple scattering model in MCNP for each of the three energy straggling options described above.

7 Numerical Results and Discussion

In this section we present illustrative numerical results for energy spectra and dose distributions, comparing predications from the existing straggling model in MCNP and our new approach against analog results. Figure 7 displays the transmitted energy spectra for a 10 MeV electron beam incident on a 0.68 *cm* slab of water, equivalent to a single step. While the purely discrete model shows the anticipated artifacts (heightened by virtue of the extremely thin target layer), the accuracy of the hybrid model, on the other hand, is outstanding. The Landau straggling distribution is accurate over the higher energy part of the spectrum but displays a prolonged tail, the well known artifact resulting from the preset cut-off designed to make the mean energy loss finite.

Table 2 shows radial and axial leakages, as well as cpu times, from a cylinder of radius 0.5 *cm* and height 1.5 *cm* for a 10 MeV beam of electrons incident on axis. The accuracy of all models is exceptional for the radial and transmitted leakages, but particularly noteworthy is that a very low order purely discrete model suffices to also give very accurate results. While the same cannot be said for the backscattered or reflected current the results are nevertheless very satisfying. All problems were run on the same single processor (3GHz, Pentium 4) and MCNP was compiled using the Intel 8.0 compiler with no optimizations. From these runtimes, we see that all of the methods result in dramatic speedups over the benchmark solution and while the expense of our new method increases with increasing numbers of moments preserved, the penalty relative to sampling Landau is not excessive.

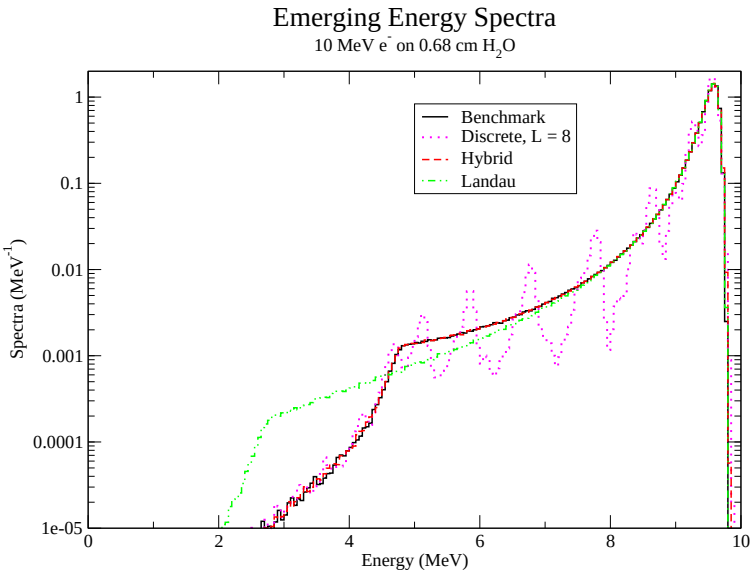

Figure 7: **Emerging Energy Spectra for** 10 **MeV** e^- **incident on a 0.68 cm slab of** H_2O

In Figure 8 we show radial dose profiles at three different locations in a cylinder of water with a radius of 5 *cm* and a height of 10 *cm*, again for a 10 MeV electron pencil beam on axis. The dose profiles were computed at $z = 1$ *cm* and $z = 4$ *cm*, with axial thickness of

Table 2: **Surface Current Tallies and Runtimes,** 10 **MeV on** H_2O **Cylinder (R=0.5 cm,Z=1.5 cm)**

Model	z=0.0 cm	z = 1.5 cm	r = 0.5 cm	Runtime
Benchmark	5.7100x10^{-5}	9.1340x10^{-1}	8.6542x10^{-2}	367.79
Landau	5.9200x10^{-5}	9.1280x10^{-1}	8.7135x10^{-2}	8.24
Disc. L=1	5.4900x10^{-5}	9.1249x10^{-1}	8.7456x10^{-2}	7.18
Disc. L=4	5.5600x10^{-5}	9.1357x10^{-1}	8.6369x10^{-2}	8.26
Disc. L=8	5.7200x10^{-5}	9.1335x10^{-1}	8.6591x10^{-2}	12.99
Hybrid	5.9300x10^{-5}	9.1351x10^{-1}	8.6426x10^{-2}	16.61

1 cm, and at $z = 8$ cm with thickness of 2 cm, and with radial cell width 0.1 cm at all locations. Once again, the accuracy of the hybrid model is uniformly outstanding, as is also the case for the standard model using Landau. The purely discrete model with four discrete energy-losses (preserving eight moments) also gives results that are barely distinguishable from the other models, while even a single discrete energy-loss model (preserving just two moments) is capable of yielding useful results.

Finally, in Figures 9, 10, and 11 we show the radial dose profiles for three different simulations, with cylinders of silicon located within a cylinder of water, similar to the above cylinder of water (i.e., a cylinder of radius 5 cm and a height of 10 cm). Also, similar to Figure 8, the radial dose profiles are of cylinders with radial cell widths of 0.1 cm and with axial thickness of 1 cm located at $z = 1$ cm and $z = 4$ cm (Figures 9 and 10), and a cylinder of axial thickness of 2 cm located at $z = 8$ cm (Figure 11). It should also be noted that these simulations were run with 10^8 electrons. Included in each figure is the benchmark for the simulation with Si in the cylinder and the appropriate approximations, and for comparison, the benchmark with H_2O in the cylinder. In Figure 9, we see the dose is primarily distributed in the center of the Si cylinder. The dose in this region is approximated with high accuracy for all of the approximate methods. It is also evident that for the purely discrete model, only four discrete energies are required to obtain an accurate approximation. Figure 10 is more interesting, as it demonstrates the effectiveness of the approximations as the electron beam spreads due to scattering. As with the previous Si cylinder, the hybrid and Landau simulations are highly accurate and indistinguishable from the benchmark. The purely discrete model, while preserving only two moments, provides even a fairly accurate approximation. Preserving 8 moments, using 4 discrete energies, provides an result that is indistinguishable from the benchmark as well. In Figure 11, we see that the beam has spread much more and much of the energy of the incident electrons has been absorbed earlier in the cylinder. Again, the Landau and the hybrid models provide excellent approximations to the benchmark. The purely discrete model, however, underestimates the dose deposited in the

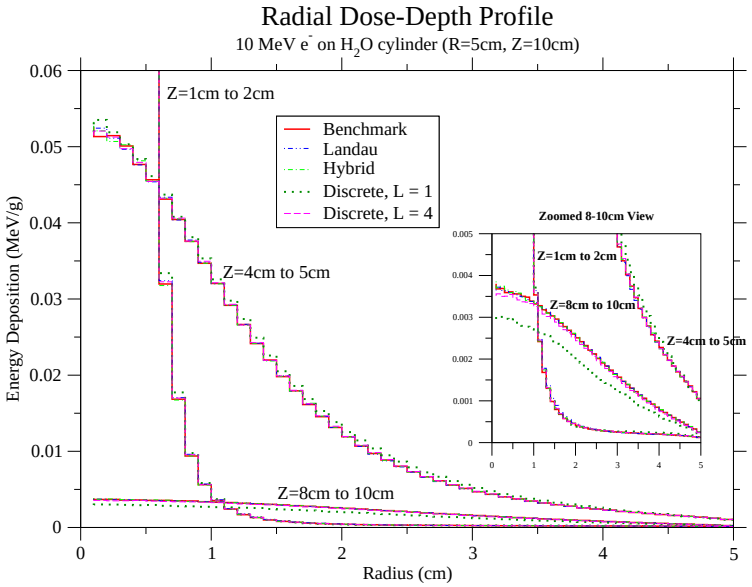

Figure 8: **Radial Dose Profile for 10 MeV e^- on H_2O Cylinder (Radius of 5 cm and Height of 10 cm, at Depths from z=1 cm to 2 cm, z=4 cm to 5 cm and z=8 cm to 10 cm)**

Si cylinder for both the $L = 1$ and $L = 4$ (which still gives a fairly accurate approximation) models. Due to the increasing accuracy obtained with increasing the number of preserved moments, by preserving 16 moments through 8 discrete energies, we are able to obtain a highly accurate solution.

8 Conclusions

We have demonstrated a new energy straggling model for use with the condensed history algorithm in MCNP. A modeled energy-loss cross section, which eliminates the singularity in the analog cross section while retaining important physical characteristics, in conjunction with a single event Monte Carlo simulation through every CH step has been shown to yield highly accurate energy spectra and dose profiles. Our method is potentially more accurate than the standard Landau straggling model with only a small increase in computational cost.

References

[1] M.J. Berger, "Monte Carlo Calculations of the Penetration and Diffusion of Fast Charged Particles," in *Methods in Computational Physics*, Vol. 1, & edited by B. Adler, S. Fernbach and M. Rotenberg, Academic Press, New York (1963).

[2] C. D. Zerby and F. L. Keller, *Nucl. Sci. Eng.*, **27**, 190 (1967).

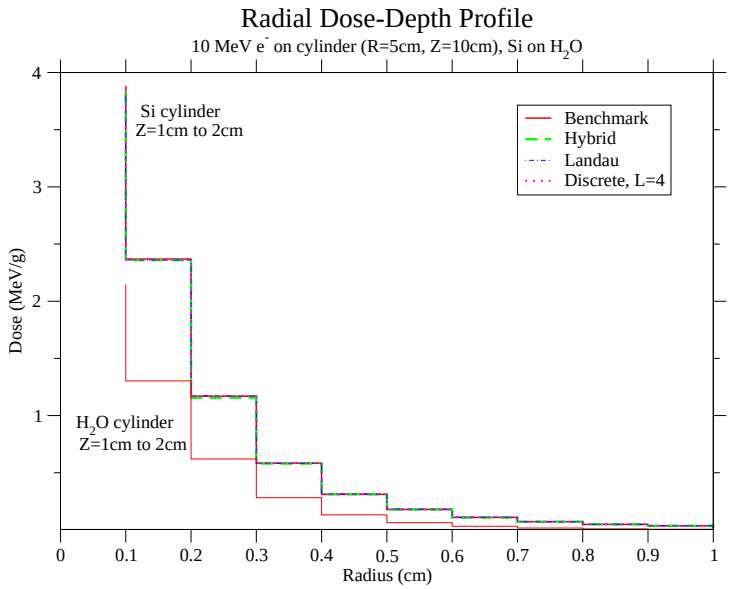

Figure 9: **Radial Dose Profile for Si Cylinder of axial thickness 1** cm **at** $z = 1$ cm **in** H_2O **Cylinder (Radius of 5 cm and Height of 10/unitscm), 10** MeV e^- **incident at** $z = 0$ cm**.**

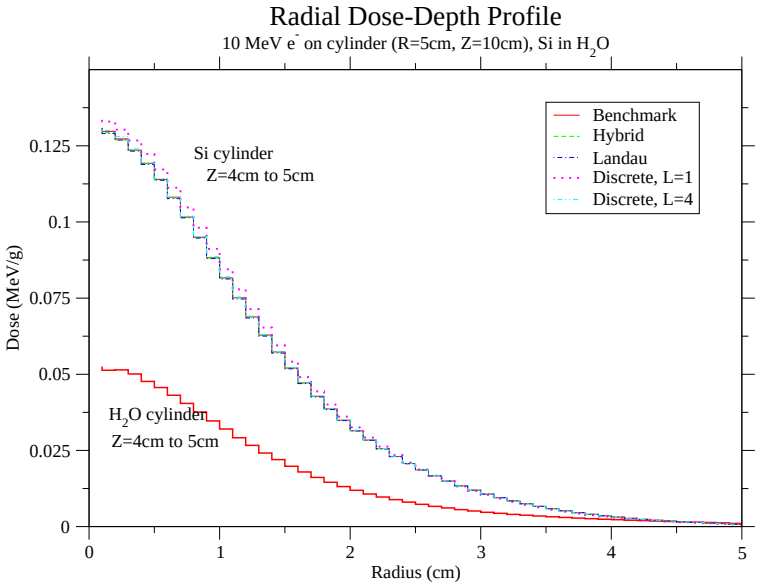

Figure 10: **Radial Dose Profile for Si Cylinder of axial thickness 1** cm **at** $z = 4$ cm **in** H_2O **Cylinder (Radius of 5 cm and Height of 10/unitscm), 10** MeV e^- **incident at** $z = 0$ cm**.**

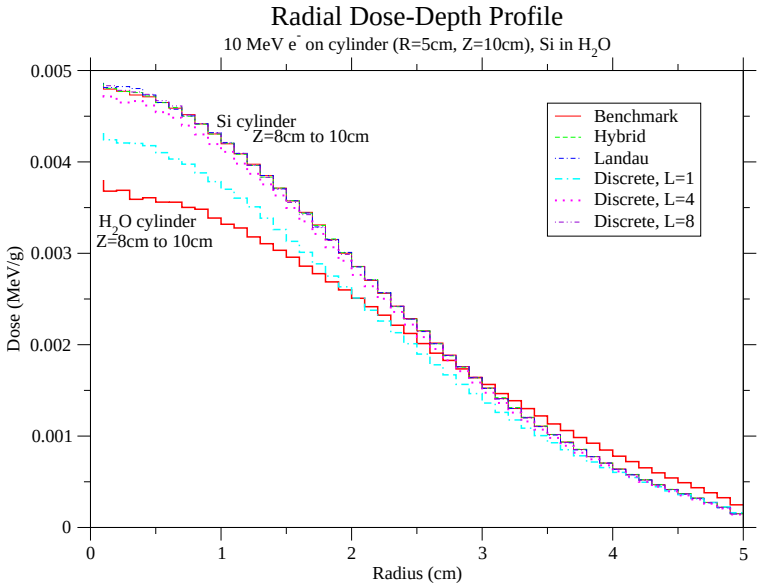

Figure 11: **Radial Dose Profile for Si Cylinder of axial thickness 2** cm **at** $z = 8$ cm **in** H_2O **Cylinder (Radius of 5 cm and Height of 10/unitscm), 10** MeV e^- **incident at** $z = 0$ cm**.**

[3] G. C. Pomraning, "Higher Order Fokker-Planck Operators," *Nucl. Sci. Eng.*, **124**, 390 (1996).

[4] A. K. Prinja and G. C. Pomraning, "A Generalized Fokker-Planck Model for Transport of Collimated Beams," *Nucl. Sci. Eng.*, **137**, 227 (2001).

[5] C. L. Leakeas and E. W. Larsen, "Generalized Fokker-Planck Approximations of Particle Transport with Highly Forward-Peaked Scattering," *Nucl. Sci. Eng.*, **137**, 236 (2001).

[6] H. W. Lewis, "Multiple Scattering in an Infinite Medium," *Phys. Rev.* **78**, 526 (1950).

[7] E. A. Straker et al., "MORSE Code: A Multigroup Neutron and Gamma-Ray Monte Carlo Transport Code," Technical Report ORNL-4716, Oak Ridge National Laboratory (1970).

[8] D. P. Sloan, "A New Multigroup Monte Carlo Scattering Algorithm for Neutral and Charged-Particle Boltzmann and Fokker-Planck Calculations," Technical Report SAND83-7094, Sandia National Laboratories (1983).

[9] J. E. Morel, L. J. Lorence, R. P. Kensek, J. A. Halbleib and D. P. Sloan, "A Hybrid Multigroup/Continuous-Energy Monte Carlo Method for Solving the Boltzmann-Fokker-Planck Equation," *Nucl. Sci. Eng.*, **124**, 369 (1996).

[10] R. Evans, *The Atomic Nucleus*, McGraw-Hill, Inc., New York (1976).

[11] S.M. Seltzer, "Electron-photon Monte Carlo Calculations: The ETRAN Code," *Appl. Radiat. Isot.*, **vol. 42, no. 10**, pp. 917-941 (1991).

[12] W. R. Nelson, H. Hirayama and D. W. O. Rogers, "The EGS4 Code System," Technical Report SLAC-265, Stanford Linear Accelerator Center (1985).

[13] J. Baró, J. Sempau, J. M. Fernandez-Varea and F. Salvat, "PENELOPE: An Algorithm for Monte Carlo Simulation of the Penetration and Energy Loss of Electrons and Positrons in Matter," *Nucl. Instr. Methods*, **B 100**, 31 (1995).

[14] X-5 MCNP Development Team, "MCNP - A General Purpose Monte Carlo N-Particle Transport Code, Version 5," *Technical Report LA-UR-03-1987*, LANL, (2003).

[15] J.A. Halbleib, R.P. Kensek, T.A. Mehlhorn, G.D. Valdez, S.M. Seltzer and M.J. Berger, "ITS version 3.0: The Integrated TIGER Series of Coupled Electron/Photon Monte Carlo," *Technical Report SAND91-1634*, SNL (1992).

[16] B. Franke and A.K. Prinja, "Monte Carlo Electron Dose Calculations using discrete angles and Discrete Energy Losses," *Nuclear Science and Engineering*, **vol. 149**, pp. 1-22 (2005).

[17] H.G. Hughes and R.E. Prael, "Modeling Charged-Particle Energy-Loss Straggling," *Technical Report LA-UR-03-3898*, LANL (2003).

[18] L.T. Harding and A.K. Prinja, "Energy-Loss Straggling for Electrons and Positrons Using Moment Preserving Methods," *Trans. Am. Nucl. Soc.*, Washington, D.C., Nov., 2005, Vol. 93, p. 453 (2005).

[19] L.T. Harding, *Monte Carlo Simulations of Electron and Positron Energy-Loss Straggling*, Master's Thesis, University of New Mexico (2005).

[20] D. R. Tolar and E. W. Larsen, "A Transport Condensed History Algorithm for Electron Monte Carlo Simulations," *Nucl. Sci. Eng.*, **139**, 47 (2001).

[21] B. C. Franke, A. K. Prinja, R. P. Kensek and L. J. Lorence, "Discrete Scattering-Angle Model for Electron Pencil Beam Transport," *Trans. Am. Nucl. Soc.*, **86**, 206 (2002).

9 Publications

1. Quirk, T., *Continuous Energy Adjoint Methods for Electron Transport*, Ph.D. Thesis, Chemical and Nuclear Engineering Department, University of New Mexico, 2008.

2. Kelsey IV, C. T. and Prinja, A.K., "Coupled Multigroup Proton/Neutron Cross Sections for Deterministic Transport, *Nuclear Technology*, 168, 257 (2009).

3. Smith, P.H. and Prinja, A.K., , "An Analysis of Moment Preserving Methods for High Energy Ion Transport, Peer Reviewed CD-ROM *Proceedings of the International Conference on Mathematics, Computational Methods and Reactor Physics*, Saratoga Springs, NY, May 3-7, 2009 (ANS Publication)

4. Smith, P.H., *Analysis of Moment-Preserving Methods for Charged Particle Transport*, MS Thesis, Chemical and Nuclear Engineering Department, University of New Mexico, 2009.

5. Kelsey IV, C. T. and Prinja, A.K., "Multigroup Neutron Dose Calculations for Proton Therapy, Peer Reviewed CD-ROM *Proceedings of the International Conference on Mathematics, Computational Methods and Reactor Physics*, Saratoga Springs, NY, May 3-7, 2009 (ANS Publication)

6. Prinja, A.K., "A Theoretical Result for Moment-Preserving Approximations to the Landau/Vavilov Straggling Model, Peer Reviewed CD-ROM *Proceedings of the International Conference on Mathematics, Computational Methods and Reactor Physics*, Saratoga Springs, NY, May 3-7, 2009 (ANS Publication)

7. Kelsey IV, C. T. and Prinja, A.K., "Multigroup and Coupled Forward-Adjoint Monte Carlo Calculation Efficiencies for Secondary Neutron Doses From Proton Beams, Peer Reviewed CD-ROM *Proceedings of the International Conference on Mathematics and Computational Applied to Nuclear Science and Engineering*, Rio de Janeiro, Brazil, May 8-12 2011 (ANS Publication)

10 Invited Seminars

1. *Moment-Preserving Methods for Charged Particle Transport: A Boltzmann Generalized Fokker-Planck (BGFP) Approach* **Distinguished Guest Lecturer Seminar** , Department of Mechanical and Aerospace Engineering, UCLA, October 10, 2007.

2. *Reduced-Order Physics Models for Computationally Efficient Charged Particle Transport*, **Colloquium**, Department of Nuclear Engineering, University of California, Berkeley, February 14, 2011.